Chemistry–A European Journal
Research Article
doi.org/10.1002/chem.202203776
Chemistry Europe
European Chemical Societies Publishing
www.chemeurj.org

Oxymethylene Ether (OME) Fuel Catalyst Screening Using In Situ NMR Spectroscopy

Patrick Endres,[a, b] Timo Schuett,[a, b] Julian Kimmig,[a, b] Stefan Zechel,[a, b] Martin D. Hager,[a, b, c] Robert Geitner,*[d] and Ulrich S. Schubert*[a, b, c]

Abstract: Online NMR measurements are introduced in the current study as a new analytical setup for investigation of the oxymethylene dimethyl ether (OME) synthesis. For the validation of the setup, the newly established method is compared with state-of-the-art gas chromatographic analysis. Afterwards, the influence of different parameters, such as temperature, catalyst concentration and catalyst type on the OME fuel formation based on trioxane and dimethoxymethane is investigated. As catalysts, Amberlyst™ 15 (A15) and trifluoromethanesulfonic acid (TfOH) are utilized. A kinetic model is applied to describe the reaction in more detail. Based on these results, the activation energy (A15: 48.0 kJ mol^{-1} and TfOH: 72.3 kJ mol^{-1}) and the order in catalyst (A15: 1.1 and TfOH: 1.3) are calculated and discussed.

Introduction

During COVID-19 pandemic in 2020, a drop in global carbon dioxide emissions was observed. However, already in 2021, the highest annual CO_2-emissions ever have been reached, according to the International Energy Agency (IEA).[1] The impact of CO_2-emissions on our climate already influences ecosystems in almost every region on earth. Possible consequences are among others heat, draught or heavy precipitations.[2] With about 20%, the transportation sector is one of the greatest contributors to greenhouse gas emissions and herein, about 75% of those emissions arise from road transport.[3]

Therefore, the reduction of carbon dioxide emissions in this sector plays a crucial role in our path towards a sustainable future.[4] Besides battery electric vehicles or fuel cell technology, alternative, carbon neutral fuels can be a promising way to reduce the emission of greenhouse gases (in particular CO_2).[5] In particular, in areas in which direct electrification is challenging[6] and due to challenges concerning lithium quality and price,[7] E-fuels can be employed. A major advantage is the possible usage as drop in fuel with small or no demand-side transformation.[6] Applied as such, the emissions of internal combustion engines can directly be reduced in dependency of the share of low carbon fuel in the blend. Oxymethylene dimethyl ethers (OME) are oxygenates, which reduce NO_x emissions as well as particulate number and matter, when employed in Diesel engines.[8–10] The use as substitute or blend with fossil Diesel or Fischer-Tropsch (FT) fuels may therefore lead not only to a reduction of carbon dioxide emissions, but also to an improvement in air quality, in particular in cities.[11–13] For the synthesis of OME_n (CH_3-O-$(CH_2O)_n$-CH_3) a formaldehyde and a methyl end capping source are required.[14] In previous studies, *p*-formaldehyde[15–16] or trioxane (TRI)[17] and as latter, methanol[18] or OME_1 (DMM)[19] were employed.

The synthesis of OME fuels based on the above mentioned reagents is acid catalyzed. These catalysts include liquid acids such as sulfuric acid[20] or methanesulfonic acid[20] as well as solid acids such as ion exchange resins[21–22] or zeolites.[19,23] The reaction leads to a product mixture following a Schulz–Flory like distribution.[24] The catalytic efficiency of the material was analyzed in literature by the measurement of the equilibrium composition of the reaction mixture.[25–27] However, the reaction kinetics gained considerable interest in recent investigations.[28–31]

In order to analyze the generation of OME fuel, gas chromatography (GC) is widely applied. GC features the ability to distinguish and quantify the homologous OME_n product mixtures.[29,32–34] Due to the chemical similarity, analysis via other techniques remains challenging. Nevertheless, the time required

[a] P. Endres, T. Schuett, J. Kimmig, Dr. S. Zechel, Dr. M. D. Hager, Prof. Dr. U. S. Schubert
Laboratory of Organic and Macromolecular Chemistry (IOMC)
Friedrich Schiller University Jena
Humboldtstr. 10, 07743 Jena (Germany)
[b] P. Endres, T. Schuett, J. Kimmig, Dr. S. Zechel, Dr. M. D. Hager, Prof. Dr. U. S. Schubert
Jena Center for Soft Matter (JCSM)
Friedrich Schiller University Jena
Philosophenweg 7, 07743 Jena (Germany)
[c] Dr. M. D. Hager, Prof. Dr. U. S. Schubert
Center for Energy and Environmental Chemistry Jena (CEEC Jena)
Friedrich Schiller University Jena
Philosophenweg 7a, 07743 Jena (Germany)
E-mail: ulrich.schubert@uni-jena.de
[d] Prof. Dr. R. Geitner
Institute for Chemistry and Bioengineering
Technical University Ilmenau
Weimarer Str. 32, 98693 Ilmenau (Germany)
E-mail: robert.geitner@tu-ilmenau.de

Supporting information for this article is available on the WWW under https://doi.org/10.1002/chem.202203776

for the analysis of one sample is high compared to other methods. GC is also limited to substances which evaporate and do not degrade the column material. In particular, strong acids, for example, the mentioned sulfuric acid, which are required for the OME synthesis, need to be avoided. Therefore, additional sample preparation steps such as neutralization of the liquid acid must be performed.[20] Furthermore, in heterogenous reactions the sampling process must be taken into account. Due to the removal of a certain amount of the liquid phase, the number of possible samples per experiment is limited to some extend as the ratio between solid catalyst and liquid reaction medium is influenced.

Nuclear magnetic resonance (NMR) spectroscopy, on the contrary, delivers detailed information about the chemical structure of the analyzed substances and no sample specific calibration is required.[35] Since the development and improvement of low-frequency benchtop devices, the incorporation into a common laboratory, and also in industry, is possible.[36–37] An additional advantage is the possibility to use flow cells and, therefore, to establish an online monitoring setup, which avoids a time-consuming sampling process and has an increased resolution in terms of time.[35–36,38]

Prior to this study, kinetic investigation of the OME fuel production was mainly based on GC analysis. The OME fuel synthesis has also been analyzed via high field NMR spectroscopy measurements.[39] Nevertheless, to the best of our knowledge, no low field benchtop NMR monitoring of the OME synthesis has been performed yet. Therefore, a new analytical setup is introduced and compared to the current state-of-the art, GC analysis. Furthermore, the activity of trifluoromethanesulfonic acid and Amberlyst™ 15 as homo- and heterogenous catalysts were kinetically evaluated and directly compared applying the new methods. Finally, in order to obtain further mechanistic insights into the catalytic mechanism, the order in catalyst was investigated. Up to date, to the best of our knowledge, an order of one was assumed, but no experimental verification has been performed yet.[29]

Results and Discussion

Concept of the study: In this study, the anhydrous synthesis of OME fuels via OME_1 and TRI (Scheme 1) was investigated due to its lower tendency to form by-products like hemi-formals compared to other starting materials.[25,27] An overview of all performed experiments (**C1**-**22**) can be found in the experimental section.

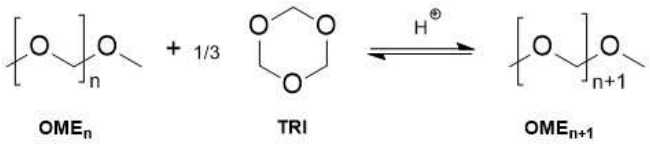

Scheme 1. Schematic representation of OME synthesis via TRI and DMM (= OME_1).

Gas chromatographic analysis was performed as previously described.[17] Molar fractions (X) were calculated based on normalized mass fractions (W) and the molar mass (M) of the components of the reaction mixture following Equation (1):

$$X_i = \frac{\frac{W_i}{M_i}}{\sum \frac{W_i}{M_i}} \quad (1)$$

To observe the reaction process *in situ*, flow NMR spectroscopy was performed. The catalyst screening setup was constructed using a 5 L double jacket reactor filled with water as heating / cooling bath. A reactor with a magnetic stirrer was placed inside. The reaction solution was in contact with a Pt100 temperature sensor monitoring the temperature of the reaction solution. Additionally, a PTFE tubing was connected to a HPLC-filter (10 μm) to prevent the solid catalyst from entering the characterization cycle. The PTFE tubing was connected to a peristaltic pump, channeling the reaction solution through the NMR spectrometer, a sampling valve for additional GC samples and back into the reactor. To compare analytical results from samples taken at the valve and the NMR measurements, a time correction was performed. This correction is required due to their different positions in the characterization cycle leading to slight deviation in the reaction observed. The time, when the reaction mixture, which was present at the time of catalyst addition, reached the corresponding station was set to zero and all further values were corrected by this time difference. The reactor setup is shown in Figure 1.

The *in situ* ^{1}H NMR spectra of the starting mixture showed three main signals, as depicted in Figure 2a. The one at about 3.75 ppm was assigned to the terminal methyl groups of the OME_1. The central methylene group revealed a signal at 3.90 ppm and the third signal was assigned to trioxane. The spectrum changed during the reaction until five main signals were detected (Figure 2b). The three above mentioned signals were again detected, although the intensity of the one linked to trioxane decreased significantly, whereas the one at 3.75 ppm is strongly overlapping with at least one additional signal, which was assigned to the terminal methylene groups of all OME_n species. The minor chemical shift variations depend on the OME chain length. The signal at 5.06 ppm is linked to the first methylene group found in OME_{2+} molecules. Compared to OME_1 the methylene groups in OME_{2+} molecules exhibit a slightly low-field shifted signal as the methylene carbon atoms experience a stronger -I-effect from the connecting oxygen atoms. Consequently, methylene groups found in the middle of the chain in OME_{3+} molecules show an even higher chemical shift at 5.20 ppm. As it can be seen from this series of ^{1}H signals the difference in shift of the methylene protons gradually gets smaller the longer the OME chains become and, thus, it was only possible to distinguish the four signals described using a low-field NMR spectrometer. As it can be seen from Figure 2 the signals change over the course of the reaction and, thus, it is possible to follow the concentration of the different species during the reaction.

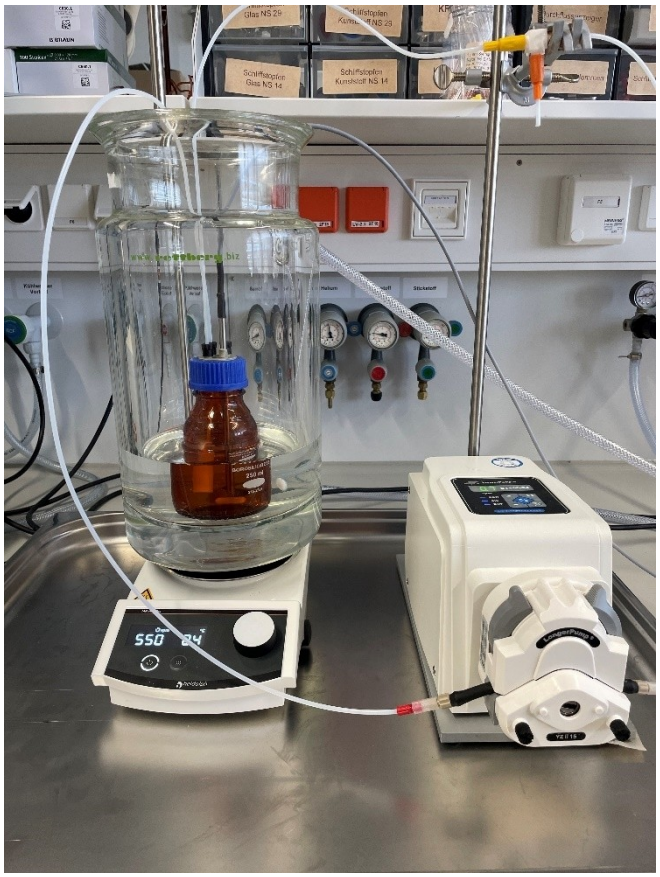

Figure 1. Picture of the reactor setup, with double jacket heating / cooling bath, reactor, peristaltic pump and PTFE-tubings connected to the NMR device.

To extract the concentrations for a kinetic analysis the signals were integrated firstly, and the NMR spectra were subsequently normalized to the area of the signal at 3.65 ppm. As discussed, this signal belongs to the terminal methyl groups and, thus, the total concentration of methyl groups in the reaction mixture does not change as formaldehyde (FA) from TRI only enables a linear chain growth but no chain branching. Using the signal areas A_X it is possible to calculate the relative number of molecules n_X by normalizing the individual signals by their respective proton count p_X (see Equation (2)). The molar ratio x_X can be calculated by dividing the relative number of molecules by the total relative number of molecules according to Equation (3).

$$n_X = \frac{A_X}{p_X} \tag{2}$$

$$x_X = \frac{n_X}{\sum_i n_{X,i}} \tag{3}$$

Due to the limited number of signals in the NMR spectra only the molar ratios of OME_1, OME_{2+} and TRI can be deduced from the ^{1}H NMR spectra. The molar ratio for OME_{3+} cannot be calculated as the exact proton count for the signal at 5.20 ppm is not known and changes throughout the reaction. Finally, the concentration c_X for each of the three species can be calculated using Equation (4):

$$c_X = \frac{x_X \cdot \rho_M}{\sum_i x_{X,i} \cdot M_{X,i}} \tag{4}$$

where ϱ_M is the density of the reaction mixture and $M_{X,i}$ is the molecular mass of the *i*th species. ϱ_M was measured for different relevant mixing ratios of the reactants and was found to be 0.922 g mL^{-1} nearly independently of the mixing ratios. M_{OME2+} was calculated using the integral of the signal at 5.20 ppm as this can be utilized to calculate an average chain length r for OME_{2+} using Equation (5). The idea is to compare the number of methylene groups within the chain to the number of terminal methylene groups.

$$r = \frac{A_{5.20}/2}{A_{5.06}/4} + 2 \tag{5}$$

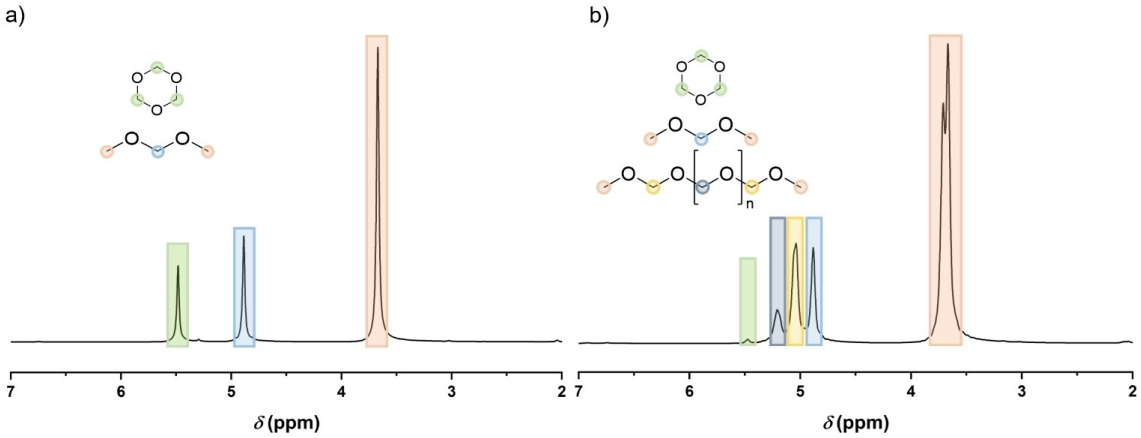

Figure 2. ^{1}H NMR spectrum of a) mixture of starting materials trioxane and DMM (43 MHz), b) product mixture with OME_{2+} (43 MHz).

Using r it is possible to calculate the average molar mass of the OME_{2+} species and, therefore, the concentrations of OME_1, OME_{2+} and TRI for each time point.

GC and NMR results

To evaluate the performance of the flow NMR spectrometer, the NMR and GC results were compared in a set of three experiments (**C1**-**3**) at 20 °C with Amberlyst™ 15 as catalyst. A molar ratio of TRI/OME_1 of 1 : 4 was applied for all three experiments and in all following experiments to ensure that all components of the reaction mixture remain dissolved. This was particularly important, as occurring precipitate could have caused complete or partial plugging of the HPLC filter.

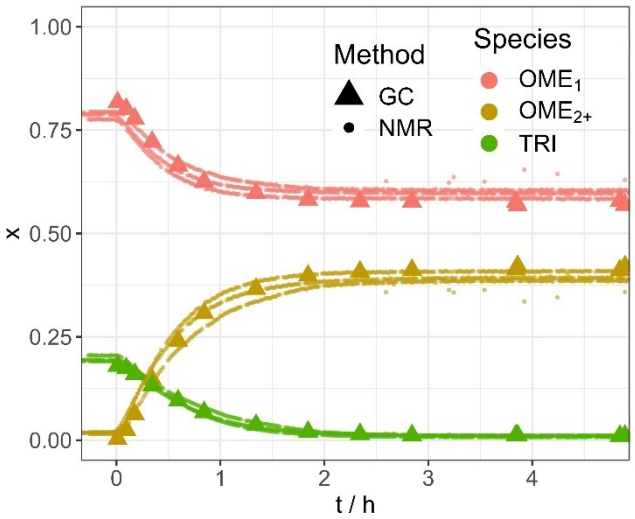

Figure 3. Molar share of OME_1, OME_{2+} and TRI over time of reactions **C1** - **3** comparing results from NMR and GC.

The determination of every OME_n (n = 1 to 10) in the product mixture was possible via GC analysis. Within this reaction, OME with a chain length up to five formed over 98 mol% of the reaction mixture and $OME_{6\text{-}10}$ were detected in traces below 1 mol%. The NMR results showed the development of OME_1, OME_{2+} and TRI over time. The results from both analysis techniques are compared in Figure 3. An extended version including the GC results up to OME_5 can be found in the Supporting Information (Figure S2). The formation of higher OMEs can be clearly observed via both analytical techniques. After a strong increase in OME_{2+} and a respective decrease of OME_1 and TRI, a slowdown of the reaction was observed. After two hours, just minor changes in the composition of the mixture were detected and a quasi-equilibrium was reached. The observed deviation between both analytical techniques is within the expected error of both methods. Therefore, online NMR measurements can be seen as highly suitable and much faster alternative compared to ex situ GC measurements. Furthermore, an experiment with phosphotungstic acid, similar to a previous literature report, revealed highly comparable results (Figure S4–S5).[41]

Kinetic evaluation

Using the online flow NMR spectrometer it was possible to follow the concentration of multiple species simultaneously with a time resolution of 60 s. This analytical power was applied to screen the influence of three important reaction parameters, namely temperature, catalyst type and catalyst concentration. The temperature was varied between 5 and 25 °C, while two catalysts (Amberlyst™ 15 and trifluoromethanesulfonic acid (TfOH)) in three different concentrations were tested. Figure 4 and 5 depict

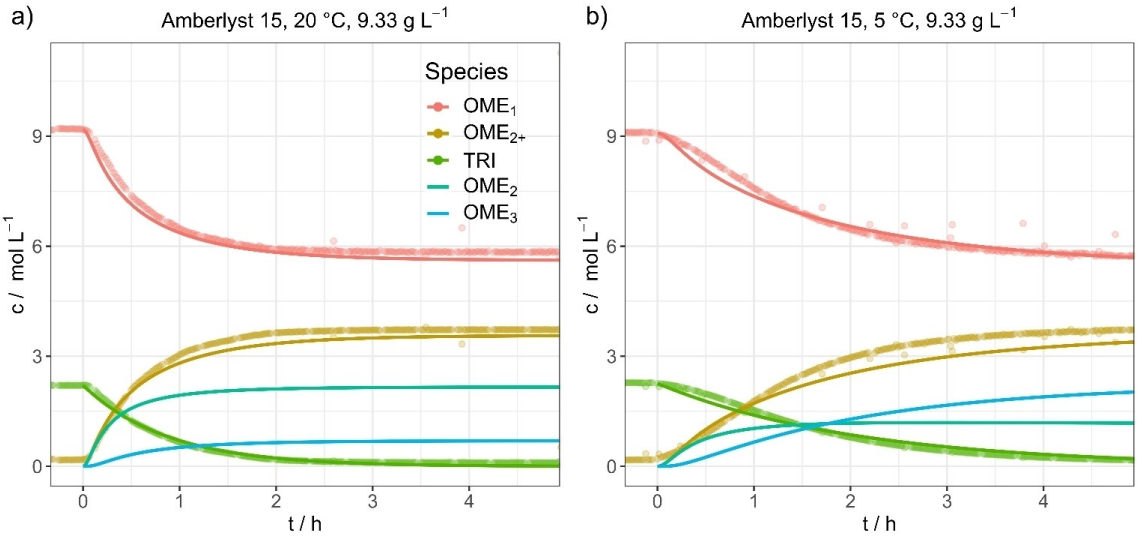

Figure 4. Experimentally extracted concentration for OME_1, OME_{2+} and TRI (dots) as well as their kinetic fits (lines). In addition to the experimentally available concentrations the fitted concentrations for OME_2 and OME_3 are shown. Reactions were performed with a) Amberlyst™ 15, 9.33 g L^{-1}, 20 °C (**C1**) b) Amberlyst™ 15, 9.33 g L^{-1}, 5 °C, (**C4**).

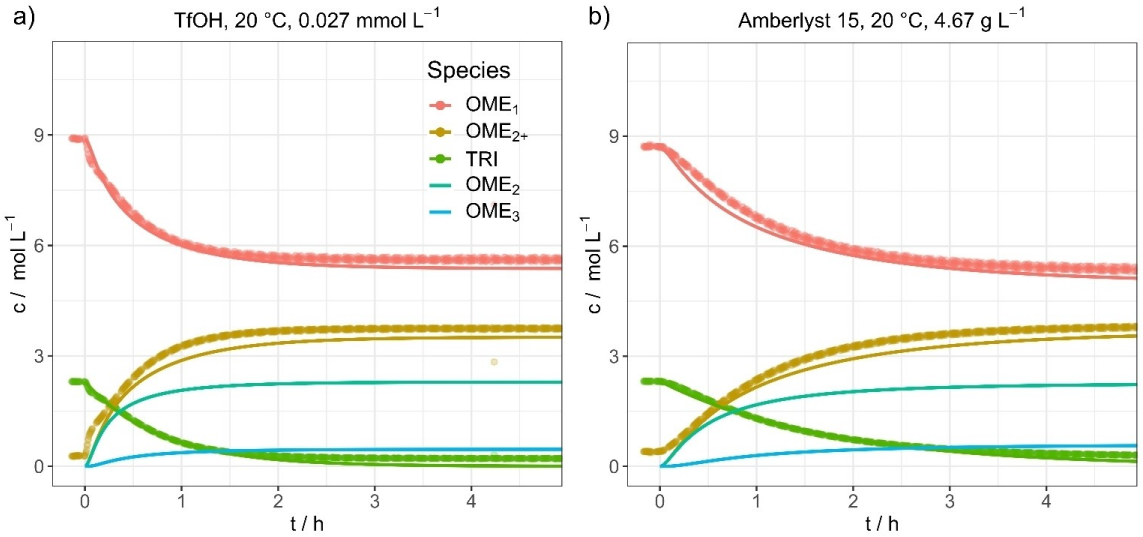

Figure 5. Experimentally extracted concentration for OME_1, OME_{2+} and TRI (dots) as well as their kinetic fits (lines). In addition to the experimentally available concentrations the fitted concentrations for OME_2 and OME_3 are shown. Reactions were performed with a) TfOH, 0.027 mol L^{-1}, 20 °C, (**C16**) b) Amberlyst™ 15, 4.67 g L^{-1}, 20 °C, (**C10**).

the influence of each parameter on the reaction rate. In Figure 4a the measured concentrations (dots) of the reaction **C1** performed with Amberlyst™ 15 with a concentration of 9.33 g L^{-1} at 20 °C are shown. After about three hours the described quasi-equilibrium was reached. By lowering the reaction temperature to 5 °C as in reaction **C4** (Figure 4b) a slowdown of the reaction rate can be observed. The equilibrium state cannot be observed within five hours leading to a decrease of the reaction rate by the factor of, at least, two. In Figure 5a the influence of the type of catalyst (**C16**) is shown. By changing from heterogeneous to homogenous catalysis, a significant increase of the reaction rate can be detected as the equilibrium state was already reached within two hours. By decreasing the catalyst amount in comparison with the first experiment (**C10**), the reaction time was prolonged significantly. As depicted in Figure 5b, the quasi-equilibrium state was again not reached within six hours although just small changes in the reaction composition were measured after five hours.

To enable a quantitative evaluation of the OME formation, a kinetic model was fitted to the experimental data. Peláez et al. described three different models to explain the reaction.[22] The first model considers all steps of the reaction as kinetically relevant and the respective reactions are seen as irreversible. The second model defines trioxane decomposition and the third model the OME propagation as rate limiting steps. As the first model was described with the least number of assumptions and, therefore, is applicable for most systems, it was chosen to serve as a kinetic model in the present study. As the GC analysis revealed that only negligible amounts of $OME_{6\text{-}10}$ were formed it was decided to model only components up to OME_5. The relevant reactions are summarized in Scheme 2 and led to the following set of differential equations which can be solved numerically.

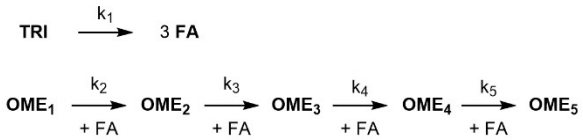

Scheme 2. Schematic representation of the relevant reactions in the OME synthesis via TRI and DMM.

$$\frac{d[TRI]}{dt} = -k_1[TRI] \tag{6a}$$

$$\frac{d[FA]}{dt} = +3k_1[TRI] - \sum_{i=2}^{5} k_i[OME_{i-1}][FA] \tag{6b}$$

$$\frac{d[OME_1]}{dt} = -k_2[OME_1][FA] \tag{6c}$$

$$\frac{d[OME_i]}{dt} = +k_i[OME_{i-1}][FA] - k_{i+1}[OME_i][FA],\ i \in \{2,\ 3,\ 4\} \tag{6d}$$

$$\frac{d[OME_5]}{dt} = +k_5[OME_4][FA] \tag{6e}$$

The data shows good accordance between the calculated and measured values. The concentrations for $OME_{2\text{-}5}$ are not directly available from the NMR measurements. Therefore, the fitted $OME_{2\text{-}5}$ concentrations were summed up and compared to the OME_{2+} concentration available from the experiments, as depicted in Figures 4 & 5. Additionally, the calculated concentrations of OME_2 and OME_3 are shown whose share is increasing as expected. Based on this fitting procedure values for the different kinetic rate constants k_1-k_5 were calculated. Following the discussion of Peláez et al. the focus was put onto k_1 as the decomposition of TRI was found to be the rate limiting step.

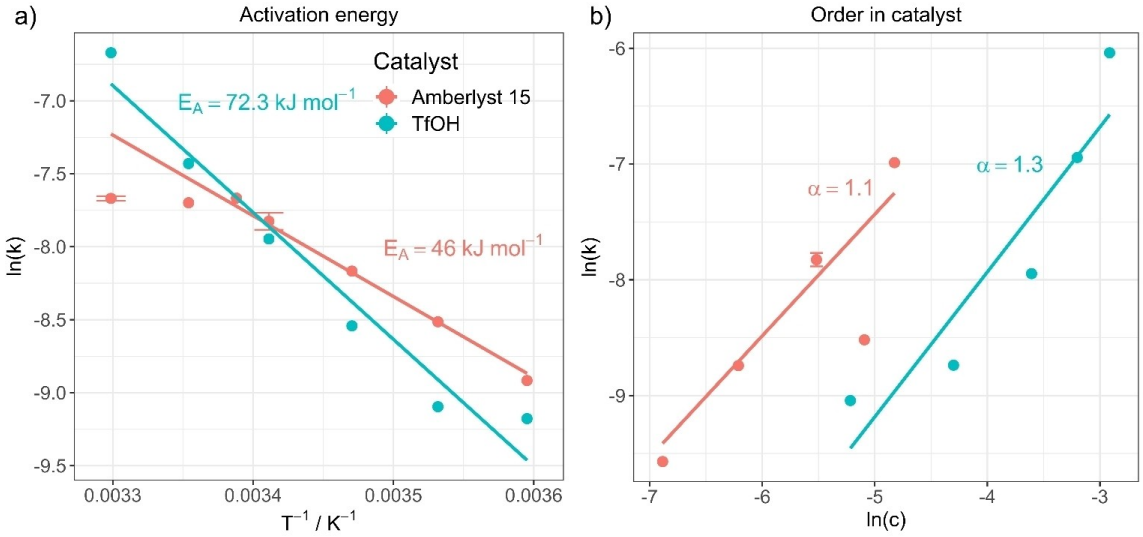

Figure 6. Arrhenius plot (a) and ln(k)-ln(c) plot (b) to extract the activation energy and order in catalyst. The error bars shown correspond to temperatures and concentrations respectively where multiple measurements were performed to evaluate the consistency of the measurement method.

Activation energy

The temperature dependent measurements enable the calculation of an activation energy for the TRI decomposition. To calculate the activation energy E_A the Arrhenius equation was applied where k is the rate constant, A the pre-exponential factor, R the universal gas constant and T the absolute temperature.

$$k = Ae^{-\frac{E_A}{RT}} \tag{7}$$

The corresponding Arrhenius plot is shown in Figure 6a. An activation energy of 46.0 kJ mol^{-1} for Amberlyst™ 15 was calculated. This value is well within the range of literature known catalysts. Examples for literature values for the OME fuel synthesis based on DMM/TRI with different acidic catalysts are summarized in Table 1. Furthermore, previous studies with depolymerization of *p*-formaldehyde with *p*-toluene sulfonic acid resulted in an activation energy of 50 kJ mol^{-1}.[40] Due to the chemical similarity of both catalyst and starting material, a comparable value can be seen as confirmation of the obtained activation energy. For TfOH the Arrhenius plot results in an E_A of 72.3 kJ mol^{-1}. This value again is within the range of expected values. The difference between both catalysts might be caused by the nature of the catalytic pathway. In heterogeneous catalysis additional effects, such as diffusion influence the reaction rate. As a consequence, a change of the reaction temperature also affects these phenomena.

Table 1. Literature known catalysts and their activation energies.

TRI cont. [mol %]	Catalyst	E_a (TRI) [kJ/mol]	E_a (OME) [kJ/mol]	Analytical technqiue
30	$H_3PW_{12}O_{40}$		82 - 99	GC [41]
30	HZSM-5[a]		28	GC [29]
12 - 29	HZSM-5[a]	57.7	51.9 - 53.1	GC [42]
23	H-Beta		96.1 (E_{app})	GC [33]
56 % (in THF)	[OMIM]Cl/$ZnCl_2$[b]	60.9	45.3	GC [43]
22 - 31	BETA	25	22.9	GC [28]
30	$[BsMIM]^+$/HSO_4^- [c]	53.2	35.7 - 39.6	GC [44]
Current study				
	Amberlyst™ 15	46.3	n.b.	NMR
	TfOH	76.8	n.b.	NMR

[a] Zeolite Socony Mobil. [b] 1-(4-Sulfonic acid) butyl-3-methylimidazolium. [c] 1-Methyl-3-octylimidazolium.

Order in catalyst

In general catalysts mostly follow a first order dependency.[45] For this reaction also a linear dependency of the reaction rate on the catalyst loading was assumed in literature,[29] which would correspond to an order in catalyst of one. Nevertheless, to the best of our knowledge no experimental verification about this hypothesis was performed, although, as this might provide essential insights into the mechanism of the reaction. Therefore, triplicate reactions with different catalyst loading of both acids were performed.

To extract the order in catalyst α Equation (8) was used.

$$k = k'[Cat]^{\alpha} \tag{8}$$

where k is the rate constant extracted by the fitting procedure and k' is a rate constant independent of the catalyst concentration. For TfOH the catalyst concentration could be directly calculated from the catalyst volume, but for Amberlyst™ 15 the calculation is not straightforward. To obtain an estimate of acidic sites in Amberlyst™ 15 the literature value of 0.43 mol H^+/kg^{-1} was utilized.[25] Thus, the mass of A15 could be

transformed into an amount of H^+, which subsequently could be used to calculate the H^+ concentration by dividing with the total volume. Although this is a simplification of the heterogenous nature of the Amberlyst™ 15 catalyst it nevertheless enables the calculation of an order for the system. As the assumptions and according transformations are applied to each catalyst concentration identically the procedure might induce a systematic error but this would have no consequence for the calculated reaction order.

Based on the results an order in catalyst α of 1.1 for Amberlyst™ 15 and 1.3 for TfOH for the decomposition of TRI was calculated (see Figure 4b). The minor difference of A15 to the expected value lies well within the error of this method and therefore confirms the assumption of an order in catalyst of one mentioned above. Baranowski et al. also found a first-order dependency of the reaction itself for a zeolite catalyst as mentioned above.[46] On the contrary, the value of 1.3 observed with TfOH as catalyst is considerably higher than expected. This finding might hint at a cooperative mechanism. In literature, just a few experiments were performed based on liquid catalysts. However, Wang et al. proposed a mechanism for [BSMIM][HSO_4] based on DFT calculations in which the counterion played a crucial role in terms of stabilization of different transition states.[47] Furthermore, in studies on the synergy of Lewis and Brønsted acid sites two roles for the catalyst, decomposition of trioxane and insertion of formaldehyde in the OME chain, have been identified. Brønsted acid sites have proven to be required for the reaction to occur, whereas an additional increase in Lewis acid sites further promotes the reaction to some extend.[48] Therefore, the observed order in catalyst supports the assumption of more than one catalytic role of TfOH.

Conclusions

Within this study, the first online NMR screening setup for monitoring of the OME fuel synthesis was reported. The analytical approach using NMR spectroscopy was compared to GC and was established as a valid alternative for the determination of kinetic data for the components OME_1, OME_{2+} and TRI. In addition, a high sampling rate was reached without influencing the reaction conditions. Further analysis of the reaction by varying temperature or catalyst loading were utilized to calculate the activation energy as well as the order in catalyst for a homogeneous and a heterogeneous catalyzed reaction. For Amberlyst™ 15 as solid catalyst an activation energy of 46.0 kJ mol^{-1} and an order of 1.1 were obtained while for TfOH as liquid catalyst the values were 72.3 kJ mol^{-1} and 1.3, respectively. Other reports always assumed a first order dependency, which was now experimentally observed for the first time. The homogeneous system shows hints towards a cooperative role of more than one catalytic moiety, as recently discussed in literature.[47–48] With online NMR monitoring established as a powerful tool, further insights into the OME fuel synthesis are the focus of future studies.

The measurement of the order in catalysts for other active materials as well as cooperative effects and the influence of diffusion on the catalytic behavior are currently being investigated.

Experimental Section

Materials and Methods: All chemicals were used as received from TCI, Sigma Aldrich and VWR, if not otherwise stated. In situ NMR spectra were recorded using a benchtop 43 MHz Spinsolve NMR spectrometer (Magritek, Germany) running on Spinsolve version 1.18.1. As advised by the manufacturer, the spectrometer was shimmed repeatedly using 10% D_2O in H_2O. A glass capillary from the same manufacturer was inserted into the spectrometer to pump the sample solution through the NMR spectrometer with a flow rate of 1.5 mL min^{-1}. Every measurement sequence was performed in an infinite loop, starting with a shim on sample, followed by ten ^{1}H NMR spectra, each in the form of a free induction decay (FID) that was recorded every minute with a pulse length of 8.6 μs, a total acquisition time of 15 s, an acquisition delay of 20 s and a dwell time of 200 μs. This results in 32,768 data points spread across an interval from −52.77 to 65.32 ppm. The schematic representation of the measurement scripts can be found in the Supporting Information.

Gas chromatography (GC) was performed on a Shimadzu GC-2010 equipped with an FID-detector, AOC-20s autosampler and AOC-20i injector. As carrier gas helium was used and a Carl Roth, RotiTM-Cap-5 MS column (30 m length, 0.25 mm ID, 0.25 μm film thickness) was utilized for compound separation. The temperature program of the GC was set as follows: 5 min 35 °C, heating with 15 K min^{-1}, 10 min at 280 °C, FID temperature 320 °C. Data evaluation was performed using customized Python script.

The double jacket reactor was connected to a Huber Unistat Tango with a temperature range between −45 to 250 °C and an accuracy of ±0.01 °C. The thermostat was equipped with a Pt100 temperature sensor from the same supplier, monitoring the reaction temperature with a data point every five seconds. The reaction solution was pumped through the NMR-spectrometer utilizing a LP-BT100-2 J peristaltic pump from LongerPump equipped with a YZII15 pump head with three rollers. For adequate pumping, the 1/8'' PTFE tubing was substituted at the pump with a Tygon S3 E-LFL tubing (**C1**-**C8**) tubing with an inner diameter of 4.8 mm and an outer diameter of 8.0 mm.

Catalyst screening experiments: The tubing and the reactor were filled with a 20 mol% solution of trioxane (44.4 g, 0.49 mol) in formaldehyde dimethyl acetal (150 g, 1.97 mol). For the comparison with the literature,[41] an 8 mol% solution of trioxane (15 g, 0.17 mol) in formaldehyde dimethyl acetal (150 g, 1.97 mol) was used (**C22**). The jacket of the reactor and the reaction solution were heated or cooled to the respective temperature and the solution was pumped with a volume of 0.7 mL min^{-1} through the system for two minutes. Afterwards, the NMR spectrometer and the temperature monitoring were started and after an equilibration time of up to one hour the catalyst (masses as depicted in Table 2) was added to the reactor. The temperature difference between the temperature set in the Huber and measured in the reaction mixture was maximal for the measurements performed at 30 °C (28.7 °C) and 5 °C (6.2 °C). The differences in all other experiments were below 1 °C. All temperatures varied +/−0.2 °C. The monitoring was stopped after no major changes of the reaction mixture were observed (min. 2 h). In addition, for the experiments **C1**-**C3**, gas chromatographic measurements were performed. For each GC sample a SEC vial with 1 mL THF and 5 μL dodecane were weighed, a sample of about 0.2 mL was removed from the reaction via the sampling valve, added and the vial was weighed again. The weight

Table 2. Overview of all reactions performed and calculated k_1 values.

Expt.	T [°C]	Cat.	m(cat.) [g]	m(DMM) [g]	m(trioxane) [g]	n(DMM) [mol]	n(TRI) [mol]	conc.	k_1 [10^{-4} s^{-1}]
C1	20	A15	1.96	150	44.4	2.0	0.5	9.33 g L^{-1}	3.17
C2	20	A15	1.96	150	44.4	2.0	0.5	9.33 g L^{-1}	4.05
C3	20	A15	1.96	150	44.4	2.0	0.5	9.33 g L^{-1}	4.35
C4	5	A15	1.96	150	44.4	2.0	0.5	9.33 g L^{-1}	1.34
C5	10	A15	1.96	150	44.4	2.0	0.5	9.33 g L^{-1}	2.01
C6	15	A15	1.96	150	44.4	2.0	0.5	9.33 g L^{-1}	2.84
C7	20	A15	1.96	150	44.4	2.0	0.5	9.33 g L^{-1}	4.36
C8	25	A15	1.96	150	44.4	2.0	0.5	9.33 g L^{-1}	4.53
C9	20	A15	3.92	150	44.4	2.0	0.5	18.66 g L^{-1}	2.01
C10	20	A15	0.98	150	44.4	2.0	0.5	4.67 g L^{-1}	1.60
C11	20	A15	0.50	150	44.4	2.0	0.5	2.38 g L^{-1}	0.70
C12	20	A15	5.00	150	44.4	2.0	0.5	23.80 g L^{-1}	9.23
C13	5	TfOH	0.86	150	44.4	2.0	0.5	27.29 mmol L^{-1}	1.03
C14	10	TfOH	0.86	150	44.4	2.0	0.5	27.29 mmol L^{-1}	1.12
Expt.	T [°C]	Cat.	m(cat.) [g]	m(DMM) [g]	m(trioxane) [g]	n(DMM) [mol]	n(TRI) [mol]	conc.	k_1 [10^{-4} s^{-1}]
C15	15	TfOH	0.86	150	44.4	2.0	0.5	27.29 mmol L^{-1}	1.95
C16	20	TfOH	0.86	150	44.4	2.0	0.5	27.29 mmol L^{-1}	3.54
C17	25	TfOH	0.86	150	44.4	2.0	0.5	27.29 mmol L^{-1}	5.93
C18	20	TfOH	1.71	150	44.4	2.0	0.5	54.26 mmol L^{-1}	23.84
C19	20	TfOH	0.43	150	44.4	2.0	0.5	13.64 mmol L^{-1}	1.60
C20	20	TfOH	0.17	150	44.4	2.0	0.5	5.39 mmol L^{-1}	1.18
C21	20	TfOH	1.28	150	44.4	2.0	0.5	40.61 mmol L^{-1}	9.64
C22	25	$H_3PW_{12}O_{40}$	0.33	150	15	2.0	0.2	1.57 g L^{-1}	2.44

difference was used as sample mass. Single deviations of datapoints were caused by small gas bubbles entering the analytical cycle, which led to temporary broadening of the NMR signals.

NMR spectra processing: The NMR pre-processing was adapted from literature.[38] The entire data analysis process was performed using R (4.2.1).[49] The R packages from the tidyverse family were utilized to organize the data and create the figures.[50]

First the NMR FID was drift corrected by using 5% of the data points recorded at the end of the acquisition period to calculate a mean value, which was subtracted from all FID values. The k^{th} data point from the FID was multiplied with an exponential apodization function featuring a frequency of W = 1 Hz.

$$e^{-\pi \bullet W \bullet k \bullet \Delta t} \tag{9}$$

Subsequently, the FID was zero filled by adding 32,768 zeros to the end of the FID resulting in 65,536 data points, which enables the extraction of all recorded information according to the Nyquist-Shannon sampling theorem.[51–54] Finally, the complex conjugate of the processed FID was Fourier transformed using a Fast Fourier Transformation algorithm.[55–56] The resulting NMR spectrum was phase corrected using the phase correction angles ϕ_0 and ϕ_1 as well as the following equations.

$$Re'_k = Re_k \cdot \cos\left(\varphi_0 + \frac{k}{N}\varphi_1\right) + Im_k \cdot \sin\left(\varphi_0 + \frac{k}{N}\varphi_1\right) \tag{10}$$

$$Im'_k = Re_k \cdot \sin\left(\varphi_0 + \frac{k}{N}\varphi_1\right) + Im_k \cdot \cos\left(\varphi_0 + \frac{k}{N}\varphi_1\right) \tag{11}$$

where k = 0, …, N-1; Re_k and Im_k are the real and imaginary components of the kth data point, Re'_k and Im'_k are the new components after correction and N is the total number of points. ϕ_0 and ϕ_1 were manual determined for each measurement series using the graphical user interface of MestReNova (14.2.3-29241).[57] Finally, the NMR spectra were referenced to the OME methyl signal (3.67 ppm), were cropped to the region of interest between -20 and 14 ppm and the frequency axis as well as all spectra were interpolated to 0.001 ppm intervals. Afterwards, the spectra were normalized to the area of the OME methyl signal (3.39 to 4.00 ppm). The preprocessed NMR spectra were analyzed by integrating the respective signals (OME_1: 4.70 to 4.96; OME_{2+}: 4.96 to 5.14; OME_{3+}: 5.14 to 5.26; TRI: 5.33 to 5.62 ppm). Equations (2)-(5) were used to transform the signal areas into concentrations.

Kinetic analysis: The R packages FME and deSolve were used to solve the kinetic differential Equations (6a-e).[58] To fit the rate constants k_1-k_5 to the experimentally determined concentrations a cost function was defined which aimed to minimize the sum of squared residuals. The experimental and fitted OME_1 and TRI concentrations could be compared directly while the experimental OME_{2+} concentration was compared to the sum of the fitted OME_2, OME_3, OME_4 and OME_5 concentrations. The activation energies and order in catalysts were subsequently calculated using k_1, the experimental temperatures or concentrations and Equation (7) or Equation (8), respectively.

The literature data points[41] shown in Figure S5 were extracted using the WebPlotDigitizer. The time-dependent trioxane concentration c extracted from the NMR spectra were converted to a conversion rate CR using the following equation:

$$CR = 1 - \frac{c}{c_0} \tag{12}$$

where c_0 denotes the trioxane concentration at the time when the catalyst was added to the reaction mixture.

Acknowledgements

The authors would like to thank Thüringer Aufbaubank (TAB) (2021 FGI 0005), the Thuringian Ministry of Economic Affairs, Science and Digital Society (TMWWdG) (CEEC-01/2020) for

funding. TOC figure was created with Biorender.com. Open Access funding enabled and organized by Projekt DEAL.

Conflict of Interest

The authors declare no conflict of interest.

Data Availability Statement

The data that support the findings of this study are available in the supplementary material of this article.

Keywords: acidic catalysis · NMR-spectroscopy · OME fuels · online characterization · synthetic fuels

[1] IEA, **2022**.
[2] H.-O. Pörtner, D. C. Roberts, E. S. Poloczanska, K. Mintenbeck, M. Tignor, A. Alegría, M. Craig, S. Langsdorf, S. Löschke, V. Möller, A. Okem (eds.), in *Climate Change 2022: Impacts, Adaptation and Vulnerability*. Contribution of Working Group II to the Sixth Assessment Report of the Intergovernmental Panel on Climate Change (Mintenbeck, M. Tignor, A. Alegría, M. Craig, S. Langsdorf, S. Löschke, V. Möller, A. Okem) Cambridge University Press, **2022**, 3–33.
[3] https://ourworldindata.org/co2-emissions-from-transport, last access: 27.02.2023.
[4] S. Khalili, E. Rantanen, D. Bogdanov, C. Breyer, *Energies* **2019**, *12*, 3870.
[5] Z. Navas-Anguita, D. García-Gusano, D. Iribarren, *Renewable Sustainable Energy Rev.* **2019**, *112*, 11–26.
[6] F. Ueckerdt, C. Bauer, A. Dirnaichner, J. Everall, R. Sacchi, G. Luderer, *Nat. Clim. Change* **2021**, *11*, 384–393.
[7] T. P. Narins, *The Extractive Industries and Society* **2017**, *4*, 321–328.
[8] D. F. Rodríguez-Vallejo, A. Valente, G. Guillén-Gosálbez, B. Chachuat, *Sustain. Energy Fuels* **2021**, *5*, 2504–2516.
[9] M. H. H. Fechter, P. Haspel, C. Hasse, A. S. Braeuer, *Fuel* **2021**, *303*, 121274.
[10] F. Mantei, R. E. Ali, C. Baensch, S. Voelker, P. Haltenort, J. Burger, R.-U. Dietrich, N. v. d. Assen, A. Schaadt, J. Sauer, O. Salem, *Sustain. Energy Fuels* **2022**, *6*, 528–549.
[11] Z. Navas-Anguita, D. García-Gusano, J. Dufour, D. Irbarren, *Appl. Energy* **2020**, *259, 114121*.
[12] C. Hank, L. Lazar, F. Mantei, M. Ouda, R. J. White, T. Smolinka, A. Schaadt, C. Hebling, H.-M. Henning, *Sustain. Energy Fuels* **2019**, *3*, 3219–3233.
[13] J. Benajes, A. García, J. Monsalve-Serrano, S. Martínez-Boggio, *Transp. Eng.* **2020**, *1*, 100001.
[14] C. J. Baranowski, A. M. Bahmanpour, O. Kröcher, *Appl. Catal. B* **2017**, *217*, 407–420.
[15] J. Burre, D. Bongartz, A. Mitsos, *Ind. Eng. Chem. Res.* **2019**, *58*, 5567–5578.
[16] M. Ouda, F. Mantei, K. Hesterwerth, E. Bargiacchi, H. Klein, R. J. White, *React. Chem. Eng.* **2018**, *3*, 676–695.
[17] P. Endres, S. Zechel, A. Winter, M. D. Hager, U. S. Schubert, *Macromol. Chem. Phys.* **2022**, *223*, 2200020.
[18] N. Schmitz, J. Burger, H. Hasse, *Ind. Eng. Chem. Res.* **2015**, *54*, 12553–12560.
[19] L. Lautenschütz, D. Oestreich, P. Haltenort, U. Arnold, E. Dinjus, J. Sauer, *Fuel Process. Technol.* **2017**, *165*, 27–33.
[20] S. Klokic, M. Hochegger, S. Schober, M. Mittelbach, *Renewable Energy* **2020**, *147*, 2151–2159.
[21] Y. Zheng, Q. Tang, T. Wang, J. Wang, *Chem. Eng. Sci.* **2015**, *134*, 758–766.
[22] R. Peláez, P. Marín, S. Ordóñez, *J. Chem. Eng.* **2020**, *396*.
[23] A. Fink, C. H. Gierlich, I. Delidovich, R. Palkovits, *ChemCatChem* **2020**, *12*, 5710–5719.
[24] D. Wang, G. Zhu, Z. Li, C. Xia, *Fuel* **2019**, *237*, 833–839.
[25] J. Burger, E. Ströfer, H. Hasse, *Ind. Eng. Chem. Res.* **2012**, *51*, 12751–12761.
[26] H. Li, H. Song, F. Zhao, L. Chen, C. Xia, *J. Energy Chem.* **2015**, *24*, 239–244.
[27] N. Schmitz, F. Homberg, J. Berje, J. Burger, H. Hasse, *Ind. Eng. Chem. Res.* **2015**, *54*, 6409–6417.
[28] G. Liu, F. Xin, C. Cao, X. Zhang, Q. Lei, H. Chen, H. Ren, *Chem. Eng. Sci.* **2022**, *253, 117537*.
[29] X. Qin, S. Lei, X. Zhang, C. Cao, F. Xin, H. Chen, X. Zhang, Y. Yin, G. Wu, *Chin. J. Chem. Eng.* **2021**, *33*, 139–146.
[30] D. Oestreich, L. Lautenschütz, U. Arnold, J. Sauer, *Chem. Eng. Sci.* **2017**, *163*, 92–104.
[31] J. Voggenreiter, J. Burger, *Ind. Eng. Chem. Res.* **2021**, *60*, 2418–2429.
[32] G. Zhu, F. Zhao, D. Wang, C. Xia, *J. Chromatogr. A* **2017**, *1513*, 194–200.
[33] C. J. Baranowski, T. Fovanna, M. Roger, M. Signorile, J. McCaig, A. M. Bahmanpour, D. Ferri, O. Kröcher, *ACS Catal.* **2020**, *10*, 8106–8119.
[34] J. Burger, M. Siegert, E. Ströfer, H. Hasse, *Fuel* **2010**, *89*, 3315–3319.
[35] S. T. Knox, S. Parkinson, R. Stone, N. J. Warren, *Polym. Chem.* **2019**, *10*, 4774–4778.
[36] A. Friebel, E. von Harbou, K. Münnemann, H. Hasse, *Ind. Eng. Chem. Res.* **2019**, *58*, 18125–18133.
[37] D. B. Thomas Castaing-Cordier, J. Farjon, P. Giraudeau, *Ann. Rep. NMR Spectrosc.* **2021**, *103*, 191–258.
[38] T. Schuett, R. Geitner, S. Zechel, U. S. Schubert, *Macromolecules* **2021**, *54*, 9410–9417.
[39] A. Peter, S. M. Fehr, V. Dybbert, D. Himmel, I. Lindner, E. Jacob, M. Ouda, A. Schaadt, R. J. White, H. Scherer, I. Krossing, *Angew. Chem. Int. Ed.* **2018**, *57*, 9461–9464; *Angew. Chem.* **2018**, *130*, 9605–9608.
[40] R. Geitner, B. M. Weckhuysen, *Chem. Eur. J.* **2020**, *26*, 5297–5302.
[41] D. Huth, M. Rose, *Catal. Sci. Technol.* **2021**, *11*, 1974–1980.
[42] C. Cao, G. Liu, F. Xin, Q. Lei, X. Qin, Y. Yin, H. Chen, A. Ullah, *Chem. Eng. Sci.* **2022**, *248*.
[43] G. Wang, S. Zhao, H. Yao, *AIChE* **2022**, e17866.
[44] D. Wang, F. Zhao, G. Zhu, C. Xia, *J. Chem. Eng.* **2018**, *334*, 2616–2624.
[45] D. G. Blackmond, *J. Am. Chem. Soc.* **2015**, *137*, 10852–10866.
[46] C. J. Baranowski, A. M. Bahmanpour, F. Héroguel, J. S. Luterbacher, O. Kröcher, *Catal. Sci. Technol.* **2019**, *9*, 366–376.
[47] F. Wang, G. Zhu, Z. Li, F. Zhao, C. Xia, J. Chen, *J. Mol. Catal. A* **2015**, *408*, 228–236.
[48] C. J. Baranowski, M. Roger, A. M. Bahmanpour, O. Krocher, *ChemSus Chem* **2019**, *12*, 4421–4431.
[49] R. Core Team, *R: A language and environment for statistical computing. R foundation for statistical computing*, Vienna, Austria, **2020**.
[50] H. Wickham, M. Averick, J. Bryan, W. Chang, L. McGowan, R. François, G. Grolemund, A. Hayes, L. Henry, J. Hester, M. Kuhn, T. Pedersen, E. Miller, S. Bache, K. Müller, J. Ooms, D. Robinson, D. Seidel, V. Spinu, K. Takahashi, D. Vaughan, C. Wilke, K. Woo, H. Yutani, *J. Open Source Softw.* **2019**, *4*, 1686.
[51] J. M. Whittaker, *Proc. Edinb. Math. Soc.* **1928**, *1*, 169–176.
[52] V. A. Kotelnikov, *Procs. of the first all-union conference on the technological reconstruction of the communications sector and low-current engineering* **1933**, 1–19.
[53] H. Nyquist, *Trans. Am. Inst. Electr. Eng.* **1928**, *47*, 617–644.
[54] C. E. Shannon, *Proce. IRE* **1949**, *37*, 10–21.
[55] W. C. James, W. T. John, *Math. Comput.* **1965**, *19*, 297–301.
[56] M. Frigo, S. G. Johnson, *Proc. IEEE* **2005**, *93*, 216–231.
[57] Mestrelab, *MestReNova*, Mestrelab Research S. L., Santiago de Compostela, Spain, **2015**.
[58] K. Soetaert, T. Petzoldt, *J. Stat. Softw.* **2010**, *33, 3*.
[59] A. Rohatgi, WebPlotDigitizer: Version 4.6, **2022**, https://automeris.io/WebPlotDigitizer.

Manuscript received: December 2, 2022
Accepted manuscript online: March 9, 2023
Version of record online: May 2, 2023